An Innovative Adaptive LBE Technique for Real-Time Crack Characterization: An Experimental Study

M. Salucci, N. Anselmi, G. Oliveri, and A. Massa

Abstract

This document deals with the real-time retrieval of the position of a crack embedded within a conductive planar structure starting from eddy current testing (*ECT*) measurements in a non-destructive testing and evaluation (*NDT-NDE*) scenario. Towards this end, an innovative adaptive learning-by-examples (*LBE*) technique has been developed. It is based on the innovative combination of a Partial Least Squares (*PLS*) features extraction technique and an adaptive sampling strategy to generate *optimal* training sets. Such information is used to train a Support Vector Regressor (*SVR*) in order to build a fast but accurate predictor of the crack descriptors staring from previously-unseen *ECT* measurements during the *on-line* testing phase.

The proposed *LBE* inversion strategy, previously validated on numerical simulations, is here tested against real laboratory-controlled experimental data coming from the World Federation of NDE Centers (*FNDEC*) “2008 Eddy Current Benchmarks”.

1 Crack Dimensions Estimation Inside a Plate Structure (Experimental)

1.1 Description of the WFNDEC 2008 experimental test cases

The considered scenarios come from the set of laboratory-controlled experimental data of the WFNDEC 2008 measurement campaign. Two experimental configurations are considered

1. **Test case 1.a - "Internal" crack**. This configuration deals with a surface-breaking notch located in the same side of the inspecting coil;
2. **Test case 1.b - "External" crack**. This configuration deals with a surface-breaking notch located in the opposite side of the inspecting coil.

The parameters of the crack (dimensions and location) considered for both test cases are given in the following table. Two experimental configurations are considered for both the "internal" and the "external" crack:

- Test cases 1.a.i and 1.b.i deal with a crack with depth $d_0 = 40\%T$;
- Test cases 1.a.ii and 1.b.ii deal with a crack with depth $d_0 = 80\%T$.

Test case 1.a - "Internal Crack"		
	Test Case 1.a.i	Test Case 1.a.ii
Depth (d_0) [mm]	0.62 ($40\%T$)	1.24 ($80\%T$)
Length (l_0) [mm]	20.0	20.0
Width (w_0) [mm]	0.11	0.14
x-coordinate (x_0) [mm]	15.0	15.0
y-coordinate (y_0) [mm]	15.0	15.0
z-coordinate (z_0) [mm]	0.31 ($D/2$)	0.62 ($D/2$)
Test case 1.a - "External Crack"		
	Test Case 1.b.i	Test Case 1.b.ii
Depth (d_0) [mm]	0.62 ($40\%T$)	1.24 ($80\%T$)
Length (l_0) [mm]	20.0	20.0
Width (w_0) [mm]	0.11	0.14
x-coordinate (x_0) [mm]	15.0	15.0
y-coordinate (y_0) [mm]	15.0	15.0
z-coordinate (z_0) [mm]	1.24 ($T - D/2$)	0.93 ($T - D/2$)

Table 1: Crack parameters for the considered experimental test cases.

1.2 Parameters of the forward solver (fixed)

Two meta-models have been considered for the accurate modelling of both the test cases. These meta-models are used as forward solvers to numerically compute the ECT signal given a particular dimension ((d_0, l_0, w_0)) of the defect.

- **Forward solver**
  - total number of measurement points along x (i.e., across the crack): $H_x = 41$;
  - measurement step along x: $\Delta_x = 0.5$ [mm];
  - total extension of the measurement region along x: $L_x = 20.0$ [mm];
  - total number of measurement points along y (i.e., along the crack): $H_y = 57$;
  - measurement step along y: $\Delta_y = 0.5$ [mm];
  - total extension of the measurement region along y: $L_y = 28.0$ [mm];
  - total number of measurement point computed by the forward solver: $H = H_x \times H_y = 2337$;

Plate	
Thickness T	1.55 [mm]
Conductivity σ	1.06 [MS/m]
Coil	
Inner radius r_1	1.0 [mm]
Outer radius r_2	1.75 [mm]
Length l_c	2.0 [mm]
Number of turns n_t	328
Lift-off δ	0.303 [mm]
Frequency f	300.0 [KHz]

Table 2: Fixed parameters.

Parameter	**Min [mm]**	**Max [mm]**
Crack Depth d_0	0.3875	1.3175
Crack Length l_0	13.0	23.0
Crack Width w_0	0.08	0.22

Table 3: Validity ranges of the forward meta-models used for modelling both test case 1.a ("internal crack") and 1.b ("external crack").

1.3 Pre-processing of the experimental data

1.3.1 Test Case 1.a.i - "Internal Crack" ($d_0 = 0.62$ **[mm]**, $l_0 = 20$ **[mm]**, $w_0 = 0.11$ **[mm]**)

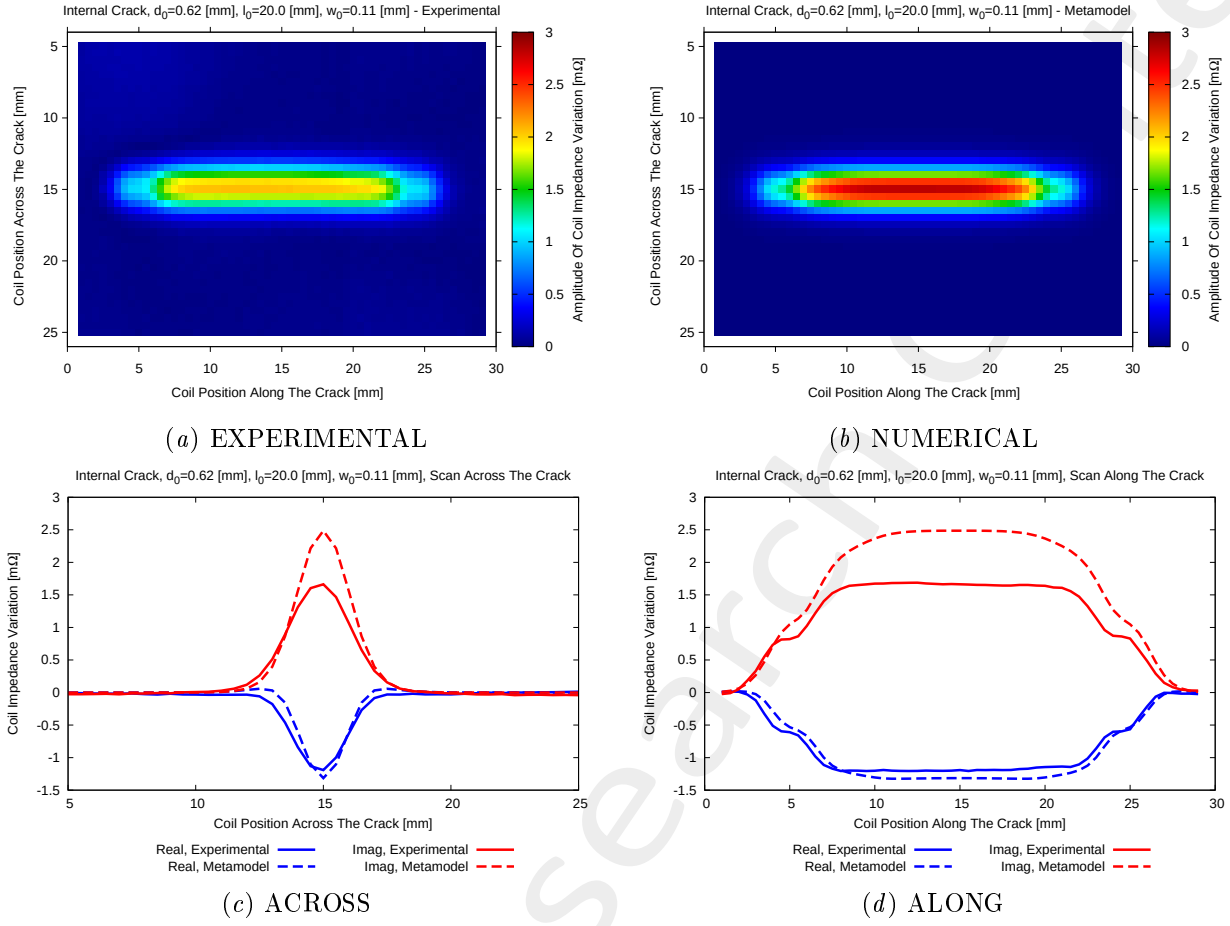

(a) EXPERIMENTAL (b) NUMERICAL

(c) ACROSS (d) ALONG

Figure 1: **Test Case 1.a.i - "Internal crack"** ($d_0 = 0.62$ **[mm]**, $l_0 = 20.0$ **[mm]**, $w_0 = 0.11$ **[mm]**) - Amplitude of the coil impedance variation for (a) the experimental and (b) the numerical signal maps. Comparison of the experimental and numerical signals measured (c) across and (d) along the crack.

1.3.2 Test Case 1.a.ii - "Internal Crack" ($d_0 = 1.24$ **[mm]**, $l_0 = 20$ **[mm]**, $w_0 = 0.14$ **[mm]**)

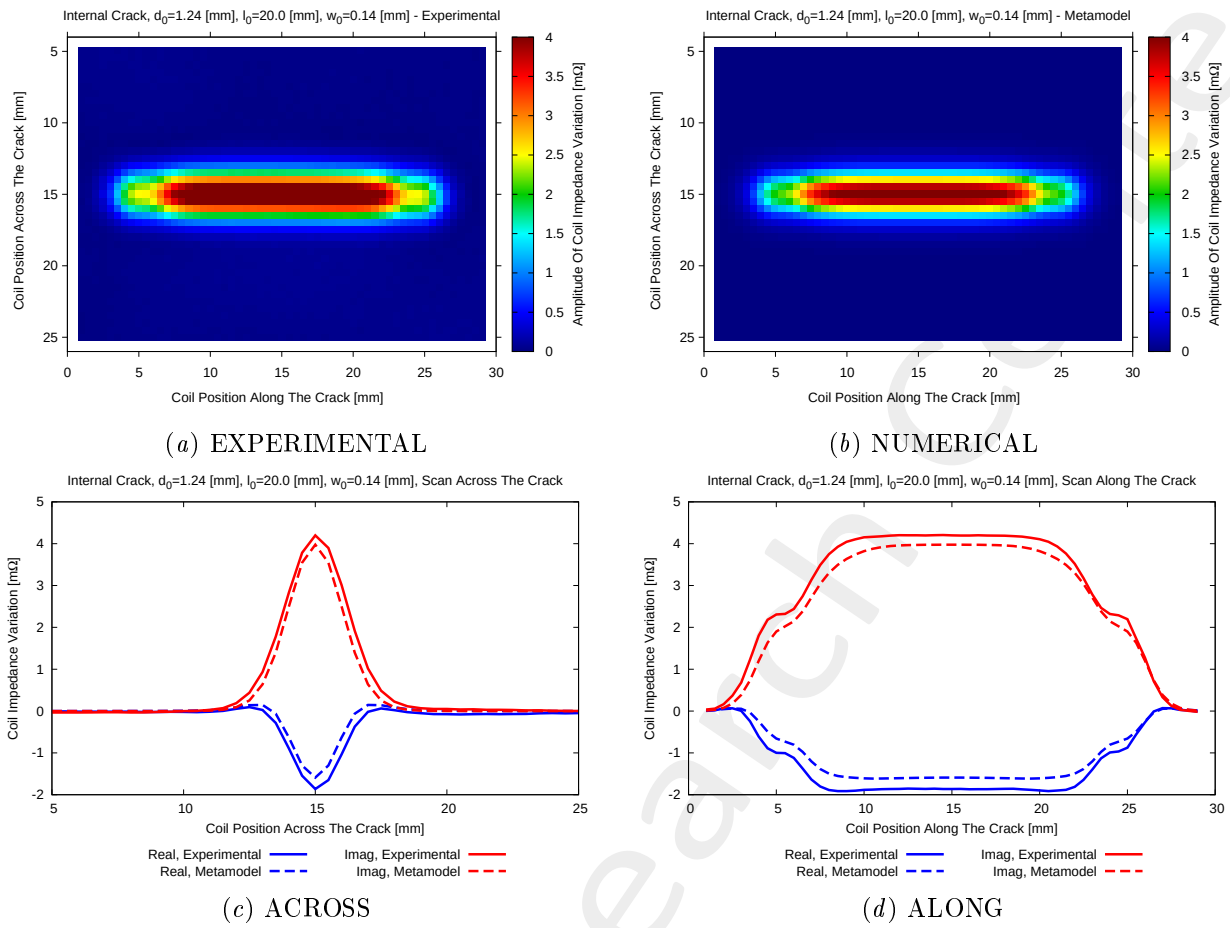

(a) EXPERIMENTAL (b) NUMERICAL

(c) ACROSS (d) ALONG

Figure 2: **Test Case 1.a.ii - "Internal crack"** ($d_0 = 1.24$ **[mm]**, $l_0 = 20.0$ **[mm]**, $w_0 = 0.14$ **[mm]**) - Amplitude of the coil impedance variation for (a) the experimental and (b) the numerical signal maps. Comparison of the experimental and numerical signals measured (c) across and (d) along the crack.

1.3.3 Test Case 1.b.i - "External Crack" ($d_0 = 0.62$ **[mm]**, $l_0 = 20$ **[mm]**, $w_0 = 0.11$ **[mm]**)

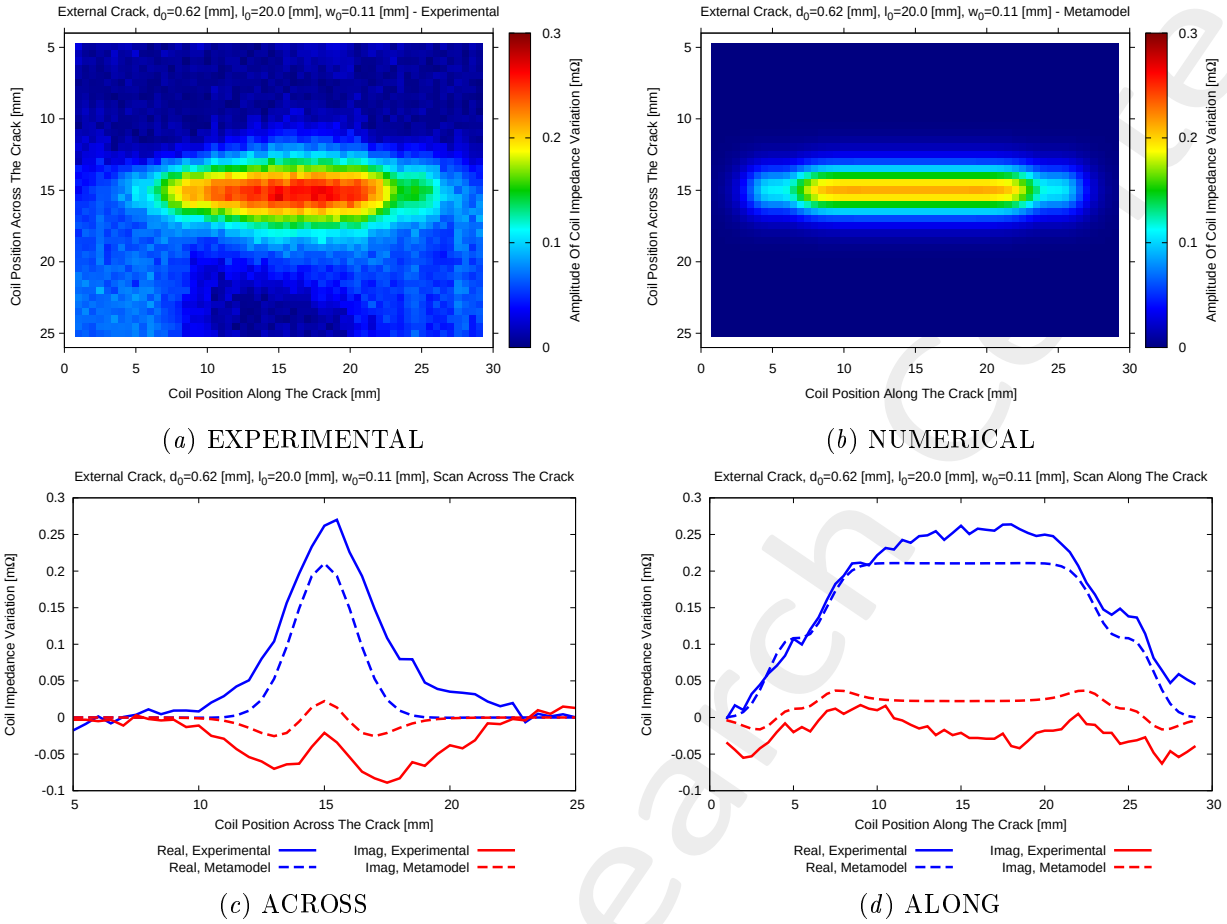

(*a*) EXPERIMENTAL (*b*) NUMERICAL

(*c*) ACROSS (*d*) ALONG

Figure 3: **Test Case 1.b.i - "External crack"** ($d_0 = 0.62$ **[mm]**, $l_0 = 20.0$ **[mm]**, $w_0 = 0.11$ **[mm]**) - Amplitude of the coil impedance variation for (*a*) the experimental and (*b*) the numerical signal maps. Comparison of the experimental and numerical signals measured (*c*) across and (*d*) along the crack.

1.3.4 Test Case 1.b.ii - "External Crack" ($d_0 = 0.62$ **[mm]**, $l_0 = 20$ **[mm]**, $w_0 = 0.11$ **[mm]**)

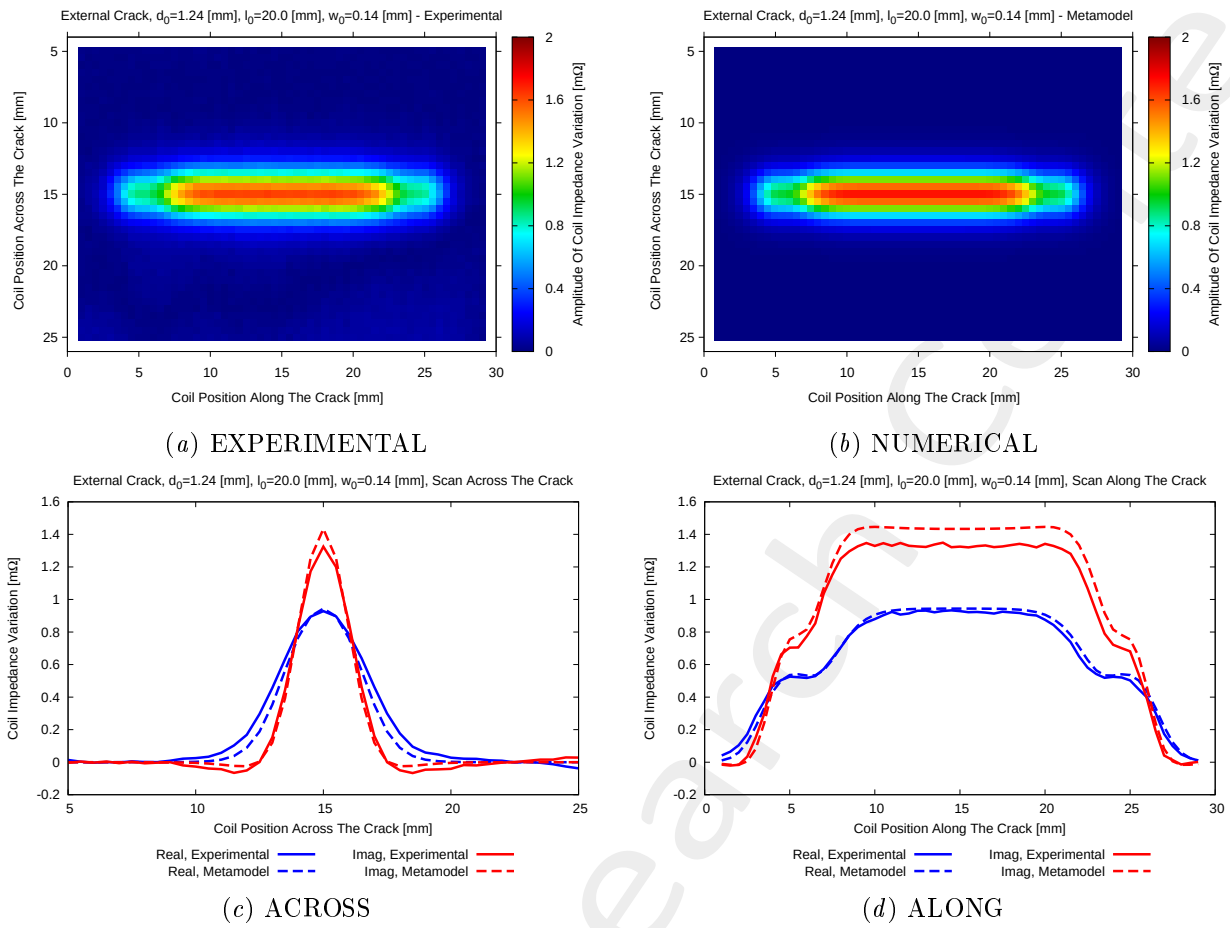

(a) EXPERIMENTAL (b) NUMERICAL

(c) ACROSS (d) ALONG

Figure 4: **Test Case 1.b.ii - "External crack"** ($d_0 = 1.24$ **[mm]**, $l_0 = 20.0$ **[mm]**, $w_0 = 0.14$ **[mm]**) - Amplitude of the coil impedance variation for (a) the experimental and (b) the numerical signal maps. Comparison of the experimental and numerical signals measured (c) across and (d) along the crack.

1.4 $PLS-OSF-SVR$ (Algorithm #3): Analysis for $J=5$ - Performances

1.4.1 Goal of this section

- Analyze performances of the $PLS-OSF-SVR$ approach when dealing with the inversion of laboratory-controlled experimental data.

1.4.2 Parameters

- **Measurement set-up for the inversion**
  - considered measurement step: $\Delta_x = \Delta_y = 0.5$ [mm];
  - number of considered measurement points $K = K_x \times K_y = 5 \times 31 = 155$;
  - measured quantity for each k-th point: $\{\Re(\Psi_k), \Im(\Psi_k)\}$;
  - total number of measured features: $F = 2 \times K = 310$;

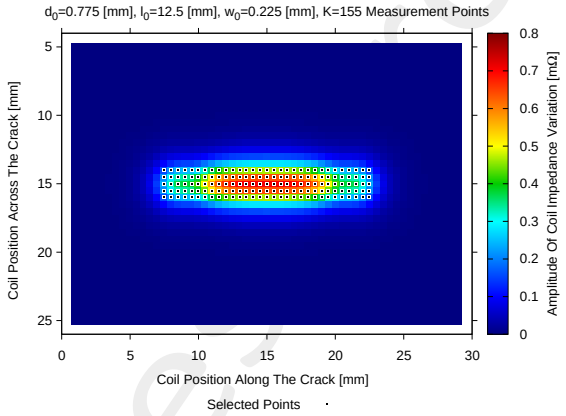

Figure 5: Location of the measurement points selected for the inversion ($K = 155$).

- $PLS-OSF-SVR$ **(algorithm #3)**
  - Initial training set (uniform grid)
    - Number of quantization levels: $Q_{d_0} = Q_{l_0} = Q_{w_0} = 5$;
    - Number of initial training samples: $N_1 = Q_{d_0} \times Q_{l_0} \times Q_{w_0} = 125$;
  - Total number of training samples: $N_{max} = 1000$;
  - Number of extracted PLS components: $J = 5$;
  - SNR on training measurements: noiseless data;
  - Number of candidate samples: $C = 150$ $(50 \times I)$ (generated via LHS sampling);
  - SNR on training data: Noiseless;

1.4.3 Results ($N = 1000$ training samples)

Test case 1.a.i			
	Actual [mm]	Predicted [mm]	Error (RE)
Depth (d_0)	0.62	0.38	38.71 %
Length (l_0)	20.0	22.50	12.5 %
Width (w_0)	0.11	0.15	36.36 %
Test case 1.a.ii			
	Actual [mm]	Predicted [mm]	Error (RE)
Depth (d_0)	1.24	1.22	1.61 %
Length (l_0)	20.0	19.90	0.5 %
Width (w_0)	0.14	0.15	7.14 %

Table 4: **Test case 1.a - "Internal Crack"** - Actual and predicted crack dimensions for the different test cases.

Test case 1.b.i			
	Actual [mm]	Predicted [mm]	Error (RE)
Depth (d_0)	0.62	0.63	1.61 %
Length (l_0)	20.0	22.50	12.5 %
Width (w_0)	0.11	0.15	36.36 %
Test case 1.b.ii			
	Actual [mm]	Predicted [mm]	Error (RE)
Depth (d_0)	1.24	1.20	3.22 %
Length (l_0)	20.0	19.63	1.85 %
Width (w_0)	0.14	0.15	7.14 %

Table 5: **Test case 1.b - "External Crack"** - Actual and predicted crack dimensions for the different test cases.

More information on the topics of this document can be found in the following list of references.

References

[1] M. Salucci, N. Anselmi, G. Oliveri, P. Calmon, R. Miorelli, C. Reboud, and A. Massa, "Real-time NDT-NDE through an innovative adaptive partial least squares SVR inversion approach," *IEEE Trans. Geosci. Remote Sens.*, vol. 54, no. 11, pp. 6818-6832, Nov. 2016 (DOI: 10.1109/TGRS.2016.2591439).

[2] M. Salucci, G. Oliveri, F. Viani, R. Miorelli, C. Reboud, P. Calmon, and A. Massa, "A learning-by-examples approach for non-destructive localization and characterization of defects through eddy current testing measurements," in *2015 IEEE International Symposium on Antennas and Propagation*, Vancouver, 2015, pp. 900-901 (DOI: 10.1109/APS.2015.7304837).

[3] M. Salucci, S. Ahmed and A. Massa, "An adaptive Learning-by-Examples strategy for efficient Eddy Current Testing of conductive structures," in *2016 European Conference on Antennas and Propagation*, Davos, 2016, pp. 1-4 (DOI: 10.1109/EuCAP.2016.7481447).

[4] P. Rocca, M. Benedetti, M. Donelli, D. Franceschini, and A. Massa, "Evolutionary optimization as applied to inverse problems," *Inverse Probl.*, vol. 25, pp. 1-41, Dec. 2009 (DOI: :10.1088/0266-5611/25/12/123003).

[5] A. Massa, P. Rocca, and G. Oliveri, "Compressive sensing in electromagnetics - A review," *IEEE Antennas Propag. Mag.*, pp. 224-238, vol. 57, no. 1, Feb. 2015 (DOI: 10.1109/MAP.2015.2397092).

[6] N. Anselmi, G. Oliveri, M. Salucci, and A. Massa, "Wavelet-based compressive imaging of sparse targets," *IEEE Trans. Antennas Propag.*, vol. 63, no. 11, pp. 4889-4900, Nov. 2015 (DOI: 10.1109/TAP.2015.2444423).

[7] M. Salucci, G. Oliveri, and A. Massa, "GPR prospecting through an inverse-scattering frequency-hopping multifocusing approach," *IEEE Trans. Geosci. Remote Sens.*, vol. 53, no. 12, pp. 6573-6592, Dec. 2015 (DOI: 10.1109/TGRS.2015.2444391).

[8] T. Moriyama, G. Oliveri, M. Salucci, and T. Takenaka, "A multi-scaling forward-backward time-stepping method for microwave imaging," *IEICE Electron. Express*, vol. 11, no. 16, pp. 1-12, Aug. 2014 (DOI: 10.1587/elex.11.20140578).

[9] T. Moriyama, M. Salucci, M. Tanaka, and T. Takenaka, "Image reconstruction from total electric field data with no information on the incident field," *J. Electromagnet. Wave.*, vol. 30, no. 9, pp. 1162-1170, 2016 (DOI: 10.1080/09205071.2016.1182876).

[10] M. Salucci, L. Poli, and A. Massa, "Advanced multi-frequency GPR data processing for non-linear deterministic imaging," *Signal Processing - Special Issue on "Advanced Ground-Penetrating Radar Signal-Processing Techniques,"* vol. 132, pp. 306-318, Mar. 2017 (DOI: 10.1016/j.sigpro.2016.06.019).